# Single-pixel PIV measurements of high-re turbulent pipe flow

Westerweel, Jerry; Sridharan, Sudarshan; Oldenziel, Gosse

**Important note**
To cite this publication, please use the final published version (if applicable).
Please check the document version above.

# SINGLE-PIXEL PIV MEASUREMENTS OF HIGH-RE TURBULENT PIPE FLOW

**Jerry Westerweel**
Laboratory for Aero & Hydrodynamics
Delft University of Technology
Mekelweg 2, 2628 CD Delft, Netherlands
j.westerweel@tudelft.nl

**Sudarshan Sridharan**
Dept. Process & Energy, Faculty 3ME
Delft University of Technology
Mekelweg 2, 2628 CD Delft, Netherlands
s.sridharan@tudelft.nl

**Gosse Oldenziel**
Deltares & Delft University of Technology
P.O. Box 177, 2600 MH Delft, The Netherlands
gosse.oldenziel@deltares.nl

## ABSTRACT

In this paper we present PIV measurements of turbulent pipe flow at Reynolds numbers between $3.4 \times 10^5$ and $6.9 \times 10^5$. We apply a so-called 'single-pixel correlation' that yields a superior spatial resolution (Westerweel *et al.*, 2004). We use the location and shape of the averaged correlation peak to obtain the mean velocity and normal and Reynolds stresses (Scharnowski *et al.*, 2012). A novel aspect of the single-pixel correlation approach is the extension to determine the spatial correlation of the velocity fluctuations. In this paper we present the results for $Re = 4.98 \times 10^5$, corresponding to a shear Reynolds number $Re_\tau = 10.3 \times 10^3$, with a spatial resolution of $\Delta y^+ = 18$.

## INTRODUCTION

One of the main limitations in obtaining experimental data of wall turbulence at very high Reynolds number is the limited spatial resolution, especially in the near-wall region. Intrusive measurement methods, such as Pitot tube and hot-wire anemometry, are limited by the dimensions of the probe. Therefore, there has been a drive to design smaller measurement probes (Vallikivi *et al.*, 2011). An alternative is to change the scale of the facility relative to the typical dimensions of the probe (Vinuesa *et al.*, 2016). Particle image velocimetry (PIV) is a non-intrusive measurement method where commonly the instantaneous flow velocity field is estimated in small interrogation regions (Adrian & Westerweel, 2011). The finite dimensions of the interrogation windows, typically $32 \times 32$ pixels, limit also the spatial resolution in the near wall region. Using an optical system with a high magnification Willert *et al.* (2017) obtained detailed measurements in the near-wall region of the CICLoPE facility, although a mirror needed to be introduced into the facility to accommodate the measurements.

Another approach is to reduce the spatial resolution of the PIV measurement to a single pixel. This approach was first described for microfluidic applications (Westerweel *et al.*, 2004), and that was later also applied to measure the mean velocity profile in the near-wall region of a turbulent boundary layer (Kähler *et al.*, 2006).

The shape of the displacement-correlation peak represents the local probability-density function for the displacement that is convoluted with the particle-image self-correlation (Westerweel, 2008). This makes it possible to estimate also the normal stresses and Reynolds stress from the measured shape of the correlation peak (Scharnowski *et al.*, 2012). However, to fully describe the turbulent flow statistics, it is necessary to also measure the local length scales. In this paper, we present a further extension to estimate the local spatial correlation of the velocity fluctuations that is based on the single-pixel algorithm.
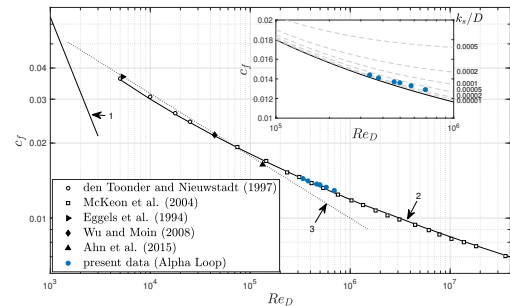


Figure 1. The friction factor $c_f$ for pipe flow as a function of the bulk Reynolds number $Re_D$. The blue dots represent the present data in the Alpha Loop. The numbered lines represent: (1) the friction factor for Poiseuille flow ($c_f = 64/Re_D$); (2) the friction law for a smooth wall (Zagarola & Smits, 1998); and (3) the Blasius friction law ($c_f = 0.316/Re_D^{1/4}$). Open symbols represent experimental data (den Toonder & Nieuwstadt, 1997; McKeon *et al.*, 2004), and closed symbols numerical data (Eggels *et al.*, 1994; Wu & Moin, 2008; Ahn *et al.*, 2015). The inset shows the present data along with lines for different values of the relative roughness $k_s/D$ according to the correlation of Colebrook (1939).

## EXPERIMENTAL SET-UP

We demonstrate this approach by measuring the turbulent flow in the 'Alpha Loop' at Deltares (Delft, The Netherlands). This facility is a closed-loop water-filled pipe with a length of 320 m and a diameter of 206 mm. The flow loop is intended for industrial-scale testing of multiphase flows, and is made of a smooth steel pipe. Measurements of were done at bulk Reynolds numbers $Re_D$ $(= U_b D/\nu)$ between $3.4{\times}10^5$ and $6.9{\times}10^5$ (where $U_b$ is the bulk velocity, $D$ is the pipe diameter, and $\nu$ the kinematic viscosity of the fluid). In Figure 1 we show the friction coefficients based on the measured pressure gradient and measured bulk flow rate. The inset of Fig. 1 shows that the pipe has a small roughness of $k_s/D = 3{\times}10^{-5}$, corresponding to $k_s = 6.2\ \mu$m.

For the PIV measurements the pipe was fitted with a transparent test section (made of PMMA) enclosed in a rectangular transparent water-filled box that can withstand the operating pressure (3 bar) and avoids serious light refraction from the curved pipe wall; a special arrangement of slits reduced internal reflections of the light sheet from the recorded images (Sridharan, 2018). The flow was seeded with 10 $\mu$m diameter tracer particles (Sphericel 110P8, Potters Inductries Inc.). The flow was illuminated with a 0.8 mm thick light sheet generated from the beam of a double-pulsed frequency-doubled dual Nd:YAG laser with a light wavelength of 532 nm. Images were recorded using a CCD camera (SensiCam QE, 1376×1040 pixels with 6.45 $\mu$m pixel pitch) equipped with a 50 mm lens (Micro Nikkor) using a $f/4$ aperture stop. The image magnification was $M_0$=0.035, ensuring ample focal depth and diffraction-limited particle images of 5.4 $\mu$m diameter. The recorded images were pre-processed using a 5×5-px min-max filter (Adrian & Westerweel, 2011) to reduce reflections that are visible in the image and normalize the image contrast (see Figure 2); this reduces the number of spurious vectors (see below) by a factor of 4-6. Any remnants of the internal reflections that occur as thin horizontal lines near the pipe walls, were removed using a Fourier filter, similar to the method for removing striations in LIF images (Westerweel *et al.*, 2011); see Fig. 2.

## SINGLE-PIXEL CORRELATION

The conventional PIV method sub-divides each image pair in small interrogation windows, of typically 32×32 pixels, and determines the local instantaneous particle-image displacement by computing the spatial correlation in typically 32×32-pixel interrogation windows, and identifying the location of the displacement-correlation peak in each interrogation window; the velocity is obtained by dividing the particle-image displacement by the exposure time-delay between the two laser light pulses that illuminate the flow (Adrian & Westerweel, 2011).

Alternatively, the particle-image displacement can be found by correlating a single pixel in the first image frame with pixels in a small domain in the second frame, and summing the correlations over many frame pairs; see Figure 3. When one uses 1024 frames, in principle the same amount of information is processed as for a single 32×32-pixel (=1024 pixels) interrogation window. However, the gain is that the spatial resolution is now determined by the dimension of a single pixel, rather than the dimension of the interrogation window; one thus improves the spatial resolution by more than an order of magnitude, at the cost of losing the ability of
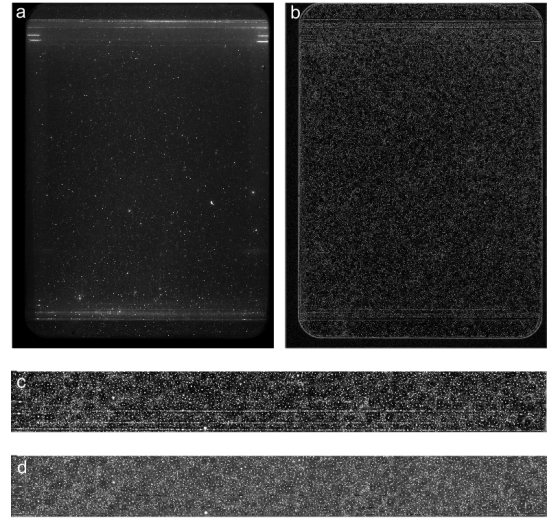


Figure 2. Image processing: (a) raw image; (b) contrast normalization by means of a 5×5-pixel min-max filter (Adrian & Westerweel, 2011); (c) detail near the lower pipe wall in image (b), and: (d) removal of remaining reflections in (c) by means of a Fourier filter (Westerweel *et al.*, 2011).
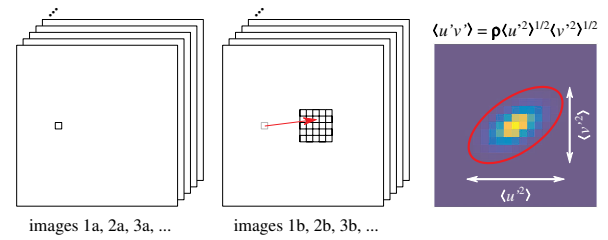


Figure 3. Principle of single-pixel PIV. For a set of image pairs the intensity at a given pixel location in the first exposure is correlated over a small region in the second exposure. The velocity is determined from the location of the displacement-correlation peak. The shape and orientation of the correlation peak yields $\langle u'^2 \rangle$, $\langle v'^2 \rangle$, and $\langle u'v' \rangle$.

recording time-resolved flows. Hence, this approach is very attractive for stationary turbulent flows where a high spatial resolution is required.

When the correlation is averaged over a sufficient number of frame pairs, it is also possible to extract the normal and Reynolds stresses from the shape and orientation of the displacement-correlation peak (Scharnowski *et al.*, 2012). The correlation peak represents the local time-averaged probability-density function of the particle-image displacements, convoluted with the particle-image self-correlation (Westerweel, 2008; Adrian & Westerweel, 2011). This self-correlation can be obtained from computing the auto-correlation of the recorded images. Then a general two-dimensional Gaussian distribution is fitted to the displacement-correlation peak, which is corrected for the convolution with the particle-image self-correlation. Finally, the normal and Reynolds stresses are obtained from the second-order moments of the remaining peak; see Figure 3 (Scharnowski *et al.*, 2012).

In this paper we introduce an extension to the single-pixel approach, and that is the evaluation of spatial correlation of
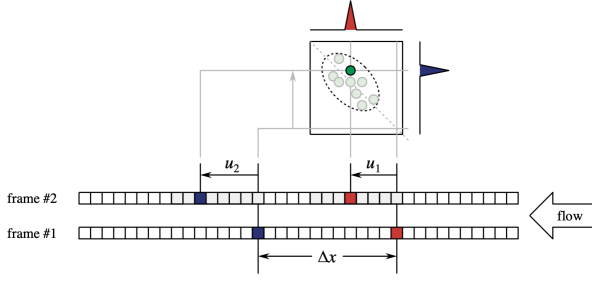
Figure 4. The estimation of the joint probability function $f(u_1, u_2|x_1, x_2)$ by the summation of single-pixel correlations at two positions separated by a distance $\Delta x$. The summation is carried out over all pixels along any homogeneous direction of the flow (here the axial direction for turbulent pipe flow) and over all recorded frames.

the velocity fluctuations. This is normally done by correlating the velocity fluctuations in two points. For a flow with a homogeneous direction, such as the axial direction in a turbulent pipe flow, the correlation is only a function of the distance $\Delta x = x_2 - x_1$. Alternatively, the correlation can be found from the joint moment of the (estimated) joint probability density function:

$$R_{uu}(\Delta x) = \overline{u'(x)u'(x+\Delta x)} = \iint u_1 u_2 f(u_1, u_2|x_1, x_2)du_1 du_2, \tag{1}$$

with: $u_1 = u'(x)$, $u_2 = u'(x+\Delta x)$, and: $\Delta x = x_2 - x_1$. Given that each single-pixel correlation for an individual frame pair is an estimate of the probability density function (pdf) $f(u,v|x)$, we multiply the pdf's at two distinct positions, and thus obtain an estimate of the joint probability density function $f(u_1, v_1, u_2, v_2|x_1, x_2)$. We now simplify this by considering a projection of the joint pdf for only one velocity component, i.e. $f(u_1, u_2|x_1, x_2)$. By averaging over a substantially large number of pixel pairs ($i$) in a large set of frame pairs, and making use of any homogeneous direction in the flow (here the axial flow direction), we can obtain a converged result from which we can estimate the spatial correlation from the joint moment of the (estimated) probability density function:

$$f(u_1, u_2|x_1, x_2) \cong \sum_i f^{(i)}(u_1|x_1) \times f^{(i)}(u_2|x_2), \tag{2}$$

as illustrated in Figure 4. Evidently, this approach only works when a particle image is present in $x_1$ and another particle image is present in $x_2$. This is why a large number of pixel pairs needs to be evaluated; by making use of a homogeneous direction in the flow—here the axial direction of the turbulent pipe flow—and summing over a large number of frames, a converged result is obtained. In the present case we have 9000 frame pairs and 900 pixels along an image line, yielding a total of more that $8 \times 10^6$ pixel pairs for each separation $\Delta x$.

## RESULTS

For each Reynolds number a total of $10^4$ double-frame images were recorded. In this paper we present the results obtained at $Re_D = 4.98 \times 10^5$ using a subset of 9000 image pairs. The corresponding shear Reynolds number $Re_\tau = 10.3 \times 10^3$, with: $Re_\tau = u_\tau R/\nu$, where $u_\tau$ is the wall friction velocity, and $R = \frac{1}{2}D$ the pipe radius.
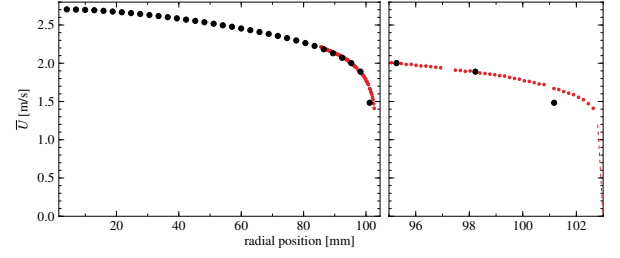


Figure 5. (left) Measured mean axial velocity profile for the lower half of the pipe. Black dots represent the conventional PIV with $32 \times 32$-pixel interrogation windows; red dots are the single-pixel correlation results. (right) Detail for the 10 mm region near the wall.
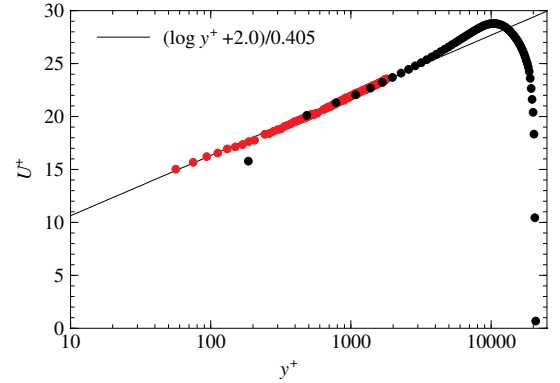


Figure 6. The mean axial velocity profile in wall units. Symbols correspond to this in Fig. 5. The first reliable measurement for conventional PIV (black dots) occurs at $y^+ = 484$ and for single-pixel PIV at $y^+ = 56$.

The $32 \times 32$-pixel interrogation result contains on average less than 1.8% spurious vectors (67 outliers per image pair yielding 3,763 vectors each, with 45 and 96 as the 5- and 95-percentiles, respectively); this indicates that there is sufficient seeding and negligible loss-of-correlation due to out-of-plane motion.

The spatial resolution of the conventional PIV is given by the dimensions of the $32 \times 32$-pixel interrogation window. For the measurement presented here this corresponds to a resolution of $\Delta y^+ \cong 600$. Evidently, this is too crude to make measurements in the near-wall region. The single-pixel approach gives a measurement at each (radial) pixel location, and thus gives a spatial resolution of $\Delta y^+ = 19$. This would in principle be sufficient to determine the flow profiles in the entire log-region. Figure 5 shows the measured velocity profiles with both the conventional and the single-pixel PIV approaches. The conventional PIV was performed over the entire flow, while the single-pixel results were only done for the near wall flow region, and ensuring a sufficient overlap with the conventional PIV data. Due to interference with remaining internal reflections, a few of the single-pixel results deviate with respect to the overall result. Figure 6 shows the same data, but now in a semi-log plot, which illustrates the high level of accuracy of the single-pixel PIV results and the extension of the range in the log-region by a decade in wall units. The profile coincides with the log profile with a von-Kármán constant of $k = 0.405$.

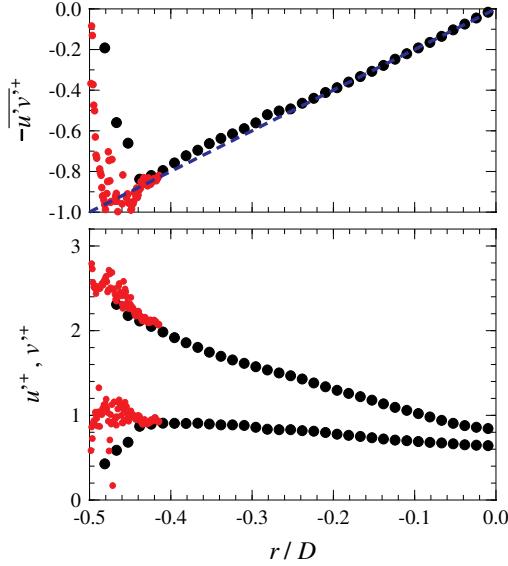Figure 7 shows the results for the normal stresses and

Figure 7. The root-mean-square turbulent fluctuation in the axial ($u'^+$) and radial ($v'^+$) directions, and Reynolds stress $-\overline{u'v'}^+$, normalized by the wall friction velocity $u_\tau$. Symbols correspond to those in Fig. 5.
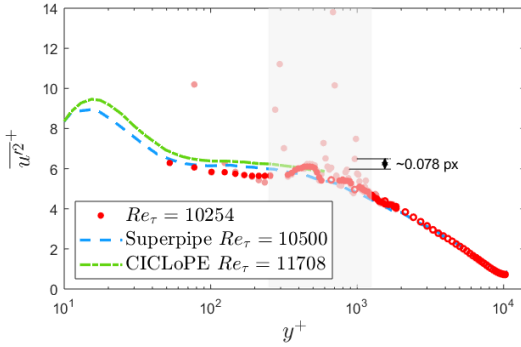


Figure 8. The streamwise normal stress $\overline{u'^2}^+$ as a function of the distance from the wall for $Re_\tau = 10.3 \times 10^3$ ($Re_D = 4.98 \times 10^3$). The red circles represent the $32 \times 32$-px PIV data, the light red dots the raw unfiltered single-pixel PIV data, and the bright red dots the median filtered single-pixel PIV data. The grey area indicates where the single pixel data is influenced by reflections. The dash-dotted green curve represents the data of Willert *et al.* (2017) for $Re_\tau = 11.7 \times 10^3$ and the dashed blue curve represents the data of Hultmark *et al.* (2013) for $Re_\tau = 10.5 \times 10^3$.

the Reynolds stress. The conventional PIV method using $32 \times 32$-pixel interrogation windows shows erroneous results for the radial normal stress and the Reynolds stress for $|r|/D > 0.43$, which corresponds to a distance $y^+ < 10^3$ from the wall. The single-pixel PIV results appears to give reliable results when approaching the wall, although the Reynolds stress results appear to give a higher noise level.

In Figure 8 the normalized normal stress $\overline{u'^2}^+$ is plotted as a function of the distance from the wall $y^+$. The data is compared with data obtained by Hultmark *et al.* (2013) at $Re_\tau = 10.5 \times 10^3$ in the Princeton Superpipe and by Willert *et al.* (2017) at $Re_\tau = 11.7 \times 10^3$ in the CICLoPE facility. The single-
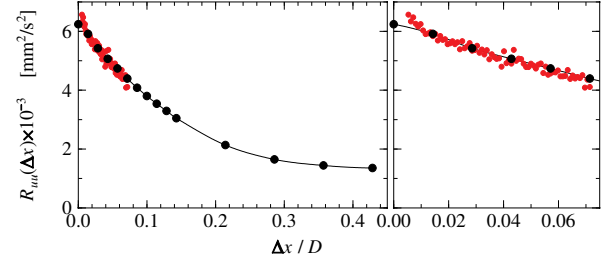


Figure 9. (left) The spatial correlation $R_{uu}(\Delta x)$ of the axial velocity fluctuations at the pipe centerline. Symbols correspond to those in Fig. 5. (right) Detail of $R_{uu}(\Delta x)$ for $\Delta x/D < 0.075$.

pixel results match the conventional $32 \times 32$-px PIV data that is available for $y^+ > 10^3$ only. The original single-pixel PIV data show some strong fluctuations for $250 < y^+ < 10^3$ (the gray region in Fig. 8). This can be attributed to the reflections that occur close to the pipe wall; see Fig. 2. By expanding the number of modes that is suppressed in the Fourier filter for images prior to the single-pixel correlation, the effect of these reflections could be substantially suppressed. The results show an acceptable agreement with the Superpipe and CICLoPE data to within an error margin that corresponds to variations in the particle-image displacement of 0.078 px (corresponding to 14 $mu$m displacement in the flow), and the plateau in $\overline{u'^2}^+$ that occurs at these high Reynolds numbers can be resolved.

In Figure 9 we present the results for the spatial correlation $R_{uu}$ of the axial velocity fluctuations at the pipe centre-line. The single-pixel result was normalised to match the tail of the spatial correlation as determined from conventional PIV data. The difference towards zero offset would indicate the result of the spatial filtering of the conventional PIV analysis. This also demonstrates the potential for single-pixel PIV to estimate the local Taylor micro-scale and dissipation rate for this type of flows from these high-resolution PIV measurements. In Figure 10 the full spatial correlation coefficient $\rho_{uu}(\Delta x)$ is shown for both the single-pixel PIV results and the conventional $32 \times 32$-px PIV results. By taking the Fourier transform of $\rho_{uu}(\Delta x)$ we find the longitudinal spectrum $F_{uu}(\kappa)$ at the centerline. The single-pixel PIV result extends the range in wavenumber by more than a decade (owing to the 16 times higher resolution compared to the conventional $32 \times 32$-px PIV data), but also becomes noisy at the higher wave numbers. By using binning over equal sections along the logarithmic axis (red dots in the bottom graph of Fig. 10) a consistent result is obtained for $\kappa D < 10^3$, whereas the conventional PIV data appears to give consistent results for $\kappa D < 150$. This demonstrates the potential of single-pixel PIV to provide information of the spatial structure of the turbulence.

## CONCLUSION

We present high-resolution PIV results (ultimately limited by the pixel size) of turbulent pipe flow, using a single-pixel PIV approach. This improves the spatial resolution by more that an order of magnitude over conventional PIV methods, while still recording the data over the full pipe diameter. This is applied to an industrial-style pipe flow facility, at shear Reynolds numbers between $Re_\tau = 7.2 \times 10^3$ and $13.9 \times 10^3$. The results presented in this paper are for the measurement at a shear Reynolds number of $Re_\tau = 10.3 \times 10^3$. Conventional PIV using $32 \times 32$-pixel interrogation windows only covers the
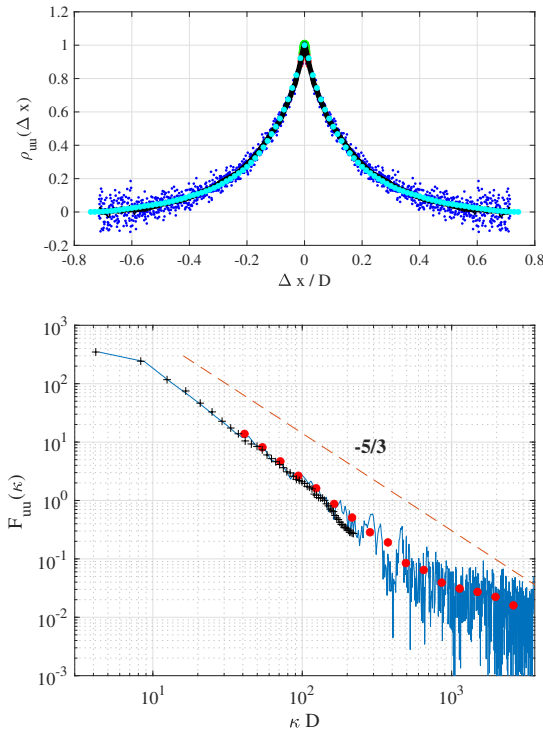
Figure 10. **(top)** The full logitudinal spatial correlation co-efficient $\rho_{uu}(\Delta x)$ for the axial velocity fluctuations at the pipe centerline. Blue dots: single-pixel correlation results; black line: same data after applying 16-px moving average filter; cyan dots: 32×32-pixel PIV result. **(bottom)** The corresponding spectrum. Blue lines: single-pixel result; red dots: binned data of single-pixel result; + symbols: 32×32-pixel PIV result.

wake region of the turbulent pipe flow, with the interrogation region closest and non-overlapping to the wall residing at the edge of the log-layer. The single-pixel PIV result is obtained by processing $10^4$ image pairs. Making use of the homogeneous axial direction in turbulent pipe flow, $8 \times 10^6$ pixel pairs are processed and resulting in a 5×5-pixel correlation peak for each radial position. Sub-pixel interpolation yields the mean velocity profile and makes it possible to resolve the full log-layer down to the buffer layer.

From the shape of the single-pixel correlation peak also the axial and radial normal stresses and the Reynolds stress can be extracted. The accuracy of the single-pixel PIV result is demonstrated by resolving the plateau in the axial normal stress that forms into an outer peak at higher Reynolds numbers. However, it appears that the result is sensitive to the presence of reflections in the image. These reflections arise from the laser light sheet that enters the optical box and inner and outer transparant pipe walls within the optical box. In the present application conventional non-fluorescent tracer particles were used; the interference of these reflections could be avoided by the use of fluorescent tracer particles in combination with an appropriate optical filter.

A novel aspect of the work is the extension of single-pixel PIV from single-point to two-point flow statistics, demonstrated by a high-resolution result for the spatial correlation of the axial velocity fluctuations. This makes it possible to obtain a reliable estimate of the turbulent spectral density for the axial velocity fluctuations.

These results were obtained with a standard PIV system with a modest resolution of 1,000 pixels. This demonstrates the capabilities of single-pixel PIV for turbulence measurements of high-Re wall turbulence, without recourse to specialized equipment or dedicated flow facilities. Using cameras with a larger format would make it possible to resolve the turbulence statistics even closer to the wall.

## REFERENCES

Adrian, R. J. & Westerweel, J. 2011 *Particle Image Velocimetry*. Cambridge University Press.

Ahn, J. Lee, J. H., Lee, J., Kang, J. & Sung, H. J. 2015 Direct numerical simulation of a 30R long turbulent pipe flow at $Re_\tau = 3008$. *Phys. Fluids* **27**, 065110.

Colebrook, C. F. 1939 Turbulent flow in pipes, with particular reference tothe transition region between smooth and rough pipe laws. *J. Inst. C. E.* **11**, 133–156.

Eggels, J. G. M., Unger, F., Weiss, M. H., Westerweel, J., Adrian, R. J., Friedrich, R. & Nieuwstadt, F. T. M. 1994 Fully developed turbulent pipe flow: a comparison between direct numerical simulation and experiment. *J. Fluid Mech.* **268**, 175–209.

Hultmark, M., Vallikivi, M., Bailey, S. C. C. & Smits, A. J. 2013 Logarithmic scaling of turbulence in smooth- and rough-wall pipe flow. *J. Fluid Mech.* **728**, 376–395.

Kähler, C. J., Scholz, U. & Ortmanns, J. 2006 Wall-shear-stress and near-wall turbulence measurements up to single pixel resolution by means of long-distance micro-PIV. *Exp. Fluids* **41**, 327–341.

McKeon, B. J., Li, J., Jiang, W., Morrison, J. F. & Smits, A. J. 2004 Further observations on the mean velocity distribution in fully developed pipe flow. *J. Fluid Mech.* **501**, 135–147.

Scharnowski, S., Hain, R. & Kähler, C. J. 2012 Reynolds stress estimation up to single-pixel resolution using PIV-measurements. *Exp. Fluids* **52**, 985–1002.

Sridharan, S. 2018 Towards high resolution particle image velocimetry. Master's thesis, Technische Universiteit Delft.

den Toonder, J. M. J. & Nieuwstadt, F. T. M. 1997 Reynolds number effects in a turbulent pipe flow for low to moderate Re. *Phys. Fluids* **9**, 3398–3409.

Vallikivi, M., Hultmark, M., Bailey, S. C. C. & Smits, A. J. 2011 Turbulence measurements in pipe flow using a nano-scale thermal anemometry probe. *Exp. Fluids* **51**, 1521–1527.

Vinuesa, R., Duncan, R. D. & Nagib, H. M. 2016 Alternative interpretation of the Superpipe data and motivation for CICLoPE: the effect of a decreasing viscous length scale. *Eur. J. Mech. B-Fluid* **58**, 109–116.

Westerweel, J. 2008 On velocity gradients in PIV interrogation. *Exp. Fluids* **44**, 831–842.

Westerweel, J., Geelhoed, P. F. & Lindken, R. 2004 Single-pixel resolution ensemble correlation for micro-PIV applications. *Exp. Fluids* **37**, 375–384.

Westerweel, J., Petracci, A., Delfos, R. & Hunt, J. C. R. 2011 Characteristics of the turbulent/non-turbulent interface of a non-isothermal jet. *Phil. Trans. R. Soc. A* **369**, 723–737.

Willert, C. E., Soria, J., Stanislas, M., Klinner, J., Amili, O., Eisfelder, M., Cuvier, C., Bellani, G., Fiorini, T. & Talamelli, A. 2017 Near-wall statistics of a turbulent pipe flow at shear Reynolds numbers up to 40 000. *J. Fluid Mech.* **826**, R5.

Wu, X. & Moin, P. 2008 A direct numerical simulation study on the mean velocity characteristics in turbulent pipe flow. *J. Fluid Mech.* **608**, 81–112.

Zagarola, M. V. & Smits, A. J. 1998 Mean-flow scaling of turbulent pipe flow. *J. Fluid Mech.* **373**, 33–79.